Influence of limestone on the hydration of ternary slag cements

Samuel Adu-Amankwah[a], Maciej Zajac[b], Christopher Stabler[b], Barbara Lothenbach[c], Leon Black[a]

[a] Institute of Resilient Infrastructure, School of Civil Engineering, University of Leeds, Woodhouse Lane, Leeds, LS2 9JT, United Kingdom

[b] HeidelbergCement Technology Center GmbH, Rohrbacher Str. 95, 69181 Leimen, Germany

[c] Empa, Laboratory for Concrete & Construction Chemistry, Überlandstrasse 129, CH-8600 Dübendorf, Switzerland

Abstract

The hydration kinetics, microstructure and pore solution composition of ternary slag-limestone cement have been investigated. Commercial CEM I 52.5 R was blended with slag and limestone; maintaining a clinker to SCM ratio of 50:50 with up to 20 % slag replaced by limestone. The sulphate content was maintained at 3 % in all composite systems. Hydration was followed by a combination of isothermal calorimetry, chemical shrinkage, scanning electron microscopy, and thermogravimetric analysis. The hydration of slag was also followed by SEM image analysis and the QXRD/PONKCS method. The accuracy of the calibrated PONKCS phase was assessed on slag and corundum mixes of varying ratios, at different water/solid ratios. Thus, the method was used to analyse hydrated cement without dehydrating the specimens. The results show that the presence of limestone enhanced both clinker and slag hydration. The pore volume and pore solution chemistry were further examined to clarify the synergistic effects. The nucleation effects account for enhanced clinker hydration while the space available for hydrate growth plus the lowering of the aluminium concentration in the pore solution led to the improved slag hydration.

Keywords:

Limestone, Hydration, PONKCS, Microstructure, Granulated blast-furnace slag

1 Introduction

Recent studies have noted synergies between alumina rich supplementary cementitious materials (SCMs) and limestone in ternary blended systems [1, 2]. This

36 interaction has the potential to maximise the respective contribution of all the
37 constituent materials [3-5] to cement performance.

38 Limestone interacts with the other components of the ternary blend in two ways; as a
39 filler and as an active reactant. As a filler, limestone increases the effective water
40 available for hydration and consequently space [6] for hydrate growth. Secondly,
41 limestone provides nucleation sites during hydration [7, 8]. Limestone is also an active
42 participant of the hydration reactions. Calcite present in limestone reacts with alumina
43 to form hemi- and monocarboaluminate phase. This results in the stabilisation of
44 ettringite [9-11], thus reducing porosity and increasing compressive strength.

45 In composite cement, the alumina content may be higher than in the neat cement
46 paste leading to increased formation of AFm phases [9-12]. This can lead to higher
47 compressive strength as previously reported for fly ash and calcined clay composite
48 cement [4, 13]. However, in slag composite cements the positive effect of limestone
49 on the strength may be counter-balanced by the formation of hydrotalcite [14, 15], thus
50 limiting the available alumina. Therefore, since demand for these cement is growing
51 [16, 17], understanding the reaction mechanisms of composite cement containing slag
52 and limestone is of high importance.

53 The impact of calcium carbonate on the hydration of ternary slag-limestone cement is
54 the focus of the present study. A multi-technique approach was applied to study
55 hydration. A PONKCS phase for GGBS was introduced in the Rietveld refinement of
56 X-ray diffraction data (XRD) obtained from freshly ground samples without hydration
57 stopping. XRD was complemented by isothermal calorimetry, chemical shrinkage,
58 thermogravimetry (TG). Additionally, samples were investigated by scanning electron
59 microscopy (SEM) equipped with energy-dispersive spectroscopy (EDS) and
60 supported by image analysis (IA). Microstructure evolution was assessed by Mercury
61 intrusion porosimetry (MIP). The observed changes in reaction kinetics and phase
62 assemblages have been related to the pore structure and pore solution chemistry
63 analysis over the course of hydration.

64 **2 Experimental details**

65 **2.1 Materials**

66 The cement investigated were prepared from commercial CEM I 52.5 R, together with
67 slag and limestone. The chemical composition and specific surface area of the
68 materials, determined by XRF and Blaine measurements respectively, is shown in
69 Table 1. The mineralogical compositions of the cement and the supplementary
70 materials are shown in Tables 2 and 3 respectively. The particle size distribution of
71 all the constituent materials, measured by laser granulometry, is shown in Figure 1.
72 The mix proportions used are detailed in Table 4.

73 The clinker to SCM ratio was maintained at 50:50, with limestone considered as an
74 SCM where incorporated. Ground anhydrite was added to the composite cement and
75 the binary quartz mix to achieve 3 % total sulphate content in each mix. The 1.9 %

76 calcite in the CEM I 52.5 R was accounted for in calculating the total limestone content
77 for the ternary blends. The formulated cements were homogenised in a laboratory ball
78 mill for at least 3 hours using polymer balls to prevent further grinding of the materials.

79

80

81

82

83 Table 1 Oxide composition of raw materials (%weight)

Material	CEM I 52.5 R [C]	Slag [S]	Limestone [L]
SiO_2	20.37	34.87	2.00
Al_2O_3	5.56	11.62	0.80
TiO_2	0.29	1.11	0.04
MnO	0.05	0.27	0.03
Fe_2O_3	2.49	0.45	0.32
CaO	62.1	41.82	53.13
MgO	1.65	5.82	0.64
K_2O	0.65	0.47	0.10
Na_2O	0.07	0.07	-
SO_3	3.54	3.13	0.07
P_2O_5	0.14	0.02	0.04
LOI	1.99	1.45	42.3
Blaine Fineness, m^2/kg	593	454	328

84

85 Table 2 Clinker content of CEM I 52.5 R (%weight)

Phase	$C_3S[M3]$	β-C_2S	C_3A	C_4AF	Calcite	Anhydrite	Bassanite	Others
Content (%)	58.1	14.3	9.2	6.7	1.9	1.7	3.0	5.1

86

87 Table 3 Mineralogical composition of supplementary materials (%weight)

Phase	Calcite	Quartz	Dolomite	Amorphous
Slag (%)	2.4	0.1	-	97.5
Limestone (%)	96.6	0.4	1	2
Quartz (%)	0.5	99.5	-	-

88   Table 4 Composition of mixes investigated (%)

Mix designation	CEM I 52.5 R	Slag/Quartz	Limestone/Quartz	Anhydrite
CS	50.68	47.08	-	2.24
CQ	51.84	48.16	-	-
CQs	50.68	47.08	-	2.24
CS-L	51.18	38.03	8.55	2.24
CS-Q	51.18	38.03	8.55	2.24
CS-2L	51.18	28.53	18.06	2.24

89   Note: The commercial CEM I 52.5 R cement contained 1.9 % calcite and 4.8 % calcium
90   sulphate, which were accounted for when maintaining a 50:50 clinker: SCM ratio.

91
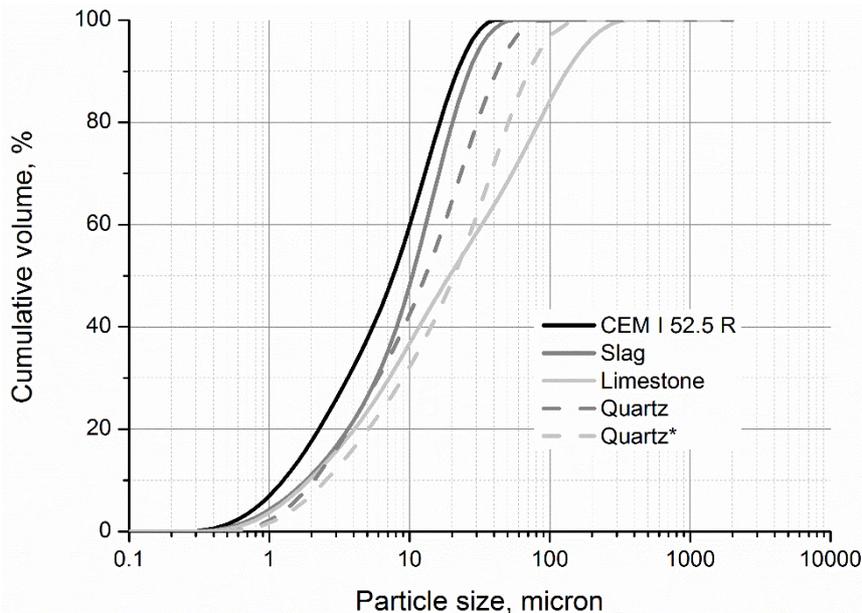
92
93   Figure 1 Particle size distribution of constituent materials, determined by laser
94   granulometry. Note: Quartz* substituted for limestone as appropriate.

2.2 Methods

96   Paste samples were prepared according to the procedure for mortar preparation, as
97   described in EN 196-1 but without aggregates. Care was taken to ensure
98   homogeneous mixing of paste by additional hand mixing.

99   The slag containing samples were investigated by the experimental program
100   comprising of a study of the hydration kinetics, pore solution concentrations and the
101   microstructure formed. Parallel measurements were performed on mixes in which slag
102   and/or limestone were replaced with quartz of similar fineness. The objective here
103   was to isolate the filler effect from the SCM reaction as elsewhere [18].

104 Isothermal calorimetry was conducted on 9.0 g of paste prepared with 0.5 w/b ratio.
105 The heat of reaction was measured continuously for 28 days at 20 $^{\circ}$C using an 8-
106 channel TAM Air calorimeter. Reference channels were filled with ampoules
107 containing 6 g of quartz mixed with 3 g of deionized water.

108 Samples for XRD, TG, MIP and SEM were cast into 15 ml plastic vials, sealed and
109 rotated for the first 12 hours to prevent bleeding. Samples were then stored in a water
110 bath until testing. XRD scans were performed on freshly ground samples aged 0.5 to
111 180 days without hydration stopping. Specimens for thermal analysis and MIP were
112 hydration stopped using a modified solvent removal technique [12], while those for
113 scanning electron microscopy (SEM) were hydration stopped by freeze-drying. The
114 solvent exchange regime involved grinding or crushing the hydrated cement into 1 –
115 2 mm particles in isopropanol (IPA) for 20 minutes, and filtering off the IPA under
116 gravity in a glove-box which was kept free of CO_2 by purging with nitrogen gas. The
117 residue was rinsed with ether before drying at 40 $^{\circ}$C on a pre-heated glass plate for 20
118 minutes. Following hydration stopping, samples were stored in mini-grip bags in the
119 glove-box until analysis.

120 XRD data were acquired on a PANalytical MPD Pro using a CuKα anode operating at
121 40 kV and 40 mA equipped with a X'Celerator detector, over a range of 5-80 $^{\circ}$2θ using
122 a step size of 0.0334 $^{\circ}$. Automatic incident divergence and fixed anti-scatter slits were
123 used together with a 10 mm incident beam mask. The continuous scan mode was
124 adopted for all data acquisition. The data analysis was performed on TOPAS
125 Academic software v4.2.

126 A first order Chebyshev polynomial background function was adopted for calibration
127 purposes. The fundamental parameter approach was used to model the slag phase.
128 This approach combined instrument and sample contributions to all peaks [19]. The
129 slag phase was modelled on a 100 % slag sample and the model is shown in Figure
130 2 together with the difference plot and peaks for the trace contents of calcite and
131 quartz.
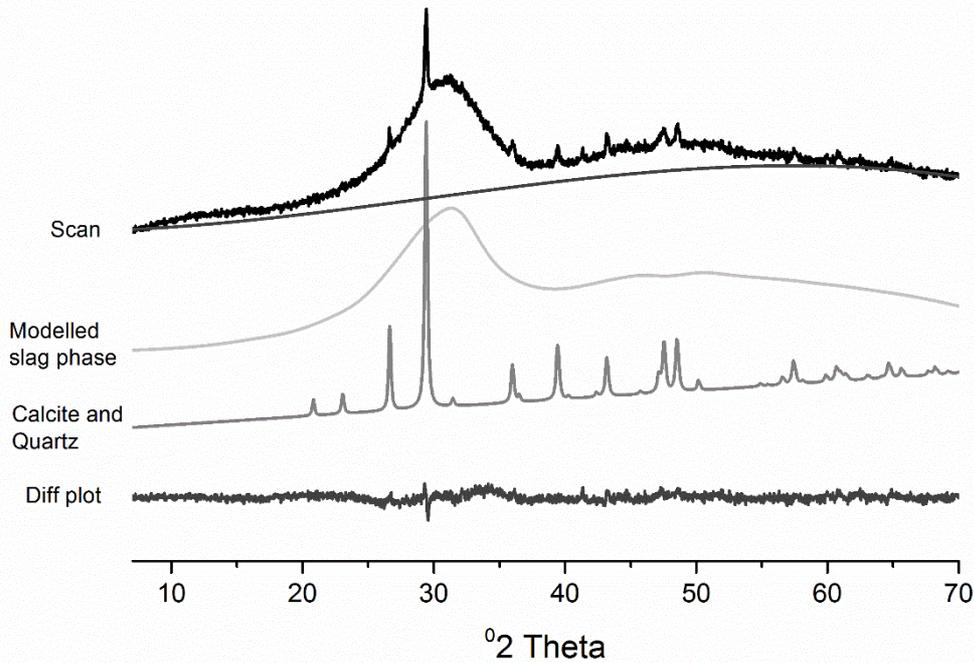
Figure 2 Modelled slag phase. From a scan of 100% slag; also shown are the difference plot and deconvoluted calcite and quartz peaks.

All instrument parameters were defined and fixed throughout the modelling and subsequent refinements. The fundamental parameter (*FP*) type peaks were introduced to describe the slag phase, taking care to avoid fitting the distinct peaks of quartz and calcite. The peaks were then indexed and refined by the Pawley method. This allowed the indexed details to be scaled together as a single *hkl* phase. The modelled slag phase was then calibrated on a 50:50 binary mix of slag and corundum. The ZM constant was determined by the internal standard method based on equation (3), taking into account the traces of quartz and calcite in the slag. The accuracy of the modelling and calibration of the slag phase was tested on binary mixes with corundum. Varying proportions of anhydrous slag and corundum were weighed, then homogenised in plastic bottles on a ball mill before scanning under the same instrument settings as for calibration.

$$(ZMV)_a = \frac{W_a}{W_{st}} \frac{S_{st}}{S_a} (ZMV)_{st} \quad ----(3)$$

Where Z is the number of formula units per unit cell, M and is mass of unit cell, V is volume per unit cell, S is scale factor, W is known weight in %, st denotes the reference standard, and a denotes the slag phase under calibration.

The effect of water addition on the binary mixes was also assessed at 0.5 and 0.3 water/solid ratios. The results are shown in Figure 3.
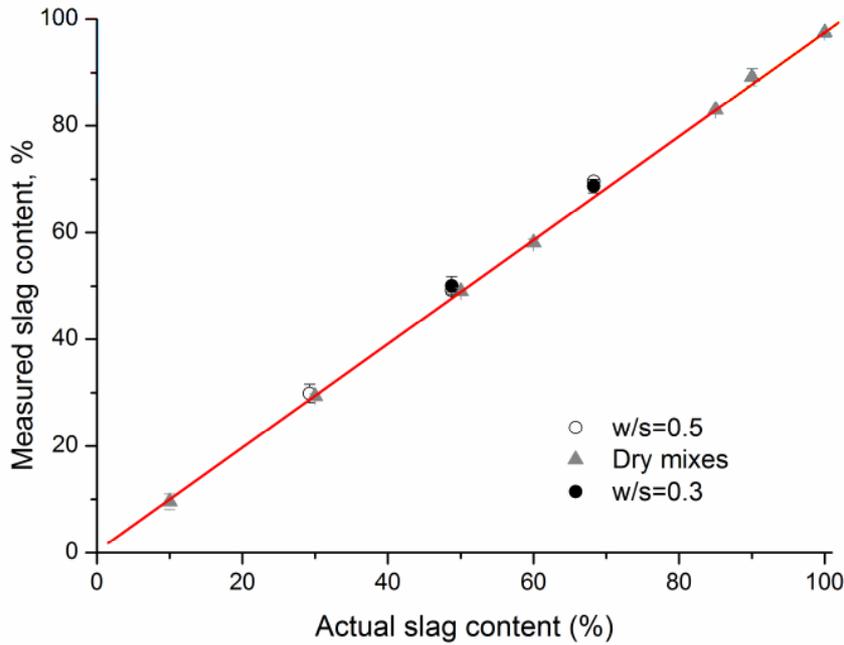
154

155 Figure 3 Relationship between actual and measured slag content. The margins of
156 error are shown as error bars. Up to 2% error can be expected; the error associated
157 with the presence of water is 0.3% and that due to changing w/s ratios is 1.8 %. These
158 are both within the measurement error.

159 The calibrated slag phase was subsequently implemented in the Rietveld refinement
160 protocol. All phases were quantified based on the external standard approach [20]
161 with corundum as the reference material. The standard was measured regularly to
162 account for the effect of tube ageing on the calibration factor [21]. A model based on
163 an *hkl* phase was implemented to account for the diffuse background contributions of
164 the free water. Following the refinement, the phase scale factors together with the
165 crystal densities, volumes and the sample mass attenuation coefficient (MAC) were
166 used to quantify the phase contents from equation (4). The G factor was similarly
167 calculated after refining the reference corundum diffraction data. The sample MAC
168 was calculated from the XRF composition and the weight fractions of the constituent
169 CEM I, SCMs, anhydrite and water in the mix. For the hydrated systems, the water
170 content used in the MAC calculation was 33.3 % of the paste since the samples were
171 not hydration stopped.   The attenuation coefficients were adopted from the
172 International Tables of Crystallography [22]. The results obtained were subsequently
173 normalised to the dry binder content.

174
$$C_a = S_a \frac{\rho_a V_a^2 \mu_{sample}}{G}$$ ------------------------- (4)

175 Where C_a is the phase content, S_a is phase scale factor, ρ_a crystal density, V_a crystal
176 volume; μ_{sample} is the sample MAC and G is the measurement calibration factor.

177 TG was carried out under nitrogen on 16-18 mg of additionally ground powder using
178 a Stanton 780 Series Analyser. The heating range was 20-1000 $^{\circ}$C at a rate of 20
179 $^{\circ}$C/minute under a flowing nitrogen atmosphere. The bound water and portlandite

180 contents were computed between 50-550 $^{\circ}$C and ~400-500 $^{\circ}$C from the TG data using
181 equations (1-2) respectively. The tangent method was used to calculate the
182 portlandite content from the TGA curves and the contents normalised to the ignited
183 weight at 550 ^{0}C according to equation 2.

184

$$\%W_n = \frac{(M_{50^{\circ}C} - M_{550^{\circ}C})}{M_{550^{\circ}C}} \ x \ 100 \text{------------------} \ (1)$$

$$\%CH = \frac{CH_w \ {}^{74}/_{18}}{M_{550^{0}C}} \ x \ 100 - - - - - - - \ (2)$$

187 Where, $\%CH$ is portlandite content, CH_w is % weight loss from water in calcium
188 hydroxide as calculated by the tangent method.

189 MIP measurements were performed on 1 – 2 mm crushed hydrated cement samples
190 using a Quantachrome Instruments' PoreMaster-60. It is noteworthy that, crushing
191 may induce micro-cracks and thus lead to potentially misleading results [23, 24].
192 However, such effects would be common to all investigated samples and hence may
193 be discounted.   Additionally, the present study focussed on the nanoscale.
194 Consequently, micrometre level defects may not interfere significantly. The pore
195 structure was characterised by the total pore volume and the threshold diameter. The
196 volume of intruded mercury was taken as the pore volume [25, 26] while the pore
197 threshold defined as the minimum diameter of connected pores was taken as the
198 intersection of the tangents to the cumulative pore volume versus pore size plot [26].

199 Samples for SEM were 2 mm thick discs cut from the paste cylinders at the required
200 age using low speed Isomet. These were resin impregnated and polished down to
201 0.25 µm using a combination of diamond paste and silicon carbide cloths. Images
202 were acquired in backscattered electron mode using a Carl Zeiss EVO MA15 equipped
203 with an 80 mm EDS detector. The instrument was operated at 15KeV accelerating
204 voltage. For the determination of the porosity, the degree of hydration of clinker and
205 slag, 50 images and their corresponding magnesium maps were obtained at 800x
206 magnification and 10 mm working distance at 2048*1536 pixel resolution for each
207 sample. Images were analysed using the ImageJ software. EDS point analysis was
208 also performed on the C-S-H and hydrated slag rim for the composition at 180 days.

209 For pore solution analysis, pastes samples were put into 200 ml (up to 1 day) or 500
210 ml (≥7 days) PE bottles, capped and sealed and stored at 20 ^{0}C. At given times, the
211 pore solutions were extracted while the specimens remained in the bottle, using
212 pressure filtration (up to 1 day) or at ≥7 days by the steel die method [27] using
213 pressures up to 250 MPa. The obtained solutions were filtered through a 0.45 µm
214 nylon filter in order to remove any remaining solids.

215 The elemental concentrations were determined by inductively coupled plasma optical
216 emission spectroscopy (ICP-OES Varian Vista-Pro). Before any measurement, the
217 solutions were filtered through a 0.45 µm nylon filter in order to remove possibly

218 remaining solids and 25 ml of solution were diluted with 5 ml HNO3 to prevent any
219 precipitation of solids. The measurements were performed not later than 1 hour after
220 pore solution extraction. For the later age samples (≥7 days), concentrations were
221 determined using a Dionex DP ICS-3000 ion chromatography. For determination of
222 solution pH, undiluted solutions were used. The pH electrode was calibrated against
223 KOH solutions of known concentrations and pH was measured directly after obtaining
224 the pore solutions.

225 Phase assemblages were modelled using GEMS (Gibbs Energy Minimisation) [28,
226 29]. Thermodynamic data was taken from the PSI– GEMS database [30] and [31]
227 along with cement specific data [32-34]. Modelling of a simplified system was
228 performed as described further in the text, to calculate the effect of limestone on the
229 pore solution concentrations.

230

231 **3 Results**

232 **3.1.0 Kinetics**

233 Isothermal conduction calorimetry gave an overview of the influence of slag and
234 limestone on the early hydration processes in ternary blended cements, as evident
235 from Figure 4. The alite reaction peak (I) was accelerated in the presence of slag and
236 even further in the limestone ternary blends, due to dilution and nucleation effects [7].
237 Double aluminate reaction peaks (II and III) were noticed in the mixes containing the
238 additional sulphate including the binary quartz mix, CQs. The first aluminate peak (II)
239 occurred after ~ 12 hours irrespective of the mix composition. This was intensified by
240 quartz in the absence of the additional anhydrite. The second aluminate peak (III),
241 was accelerated by slag. This was however retarded in the limestone ternary blends
242 irrespective of the limestone content but slightly accelerated in the quartz ternary
243 blend.
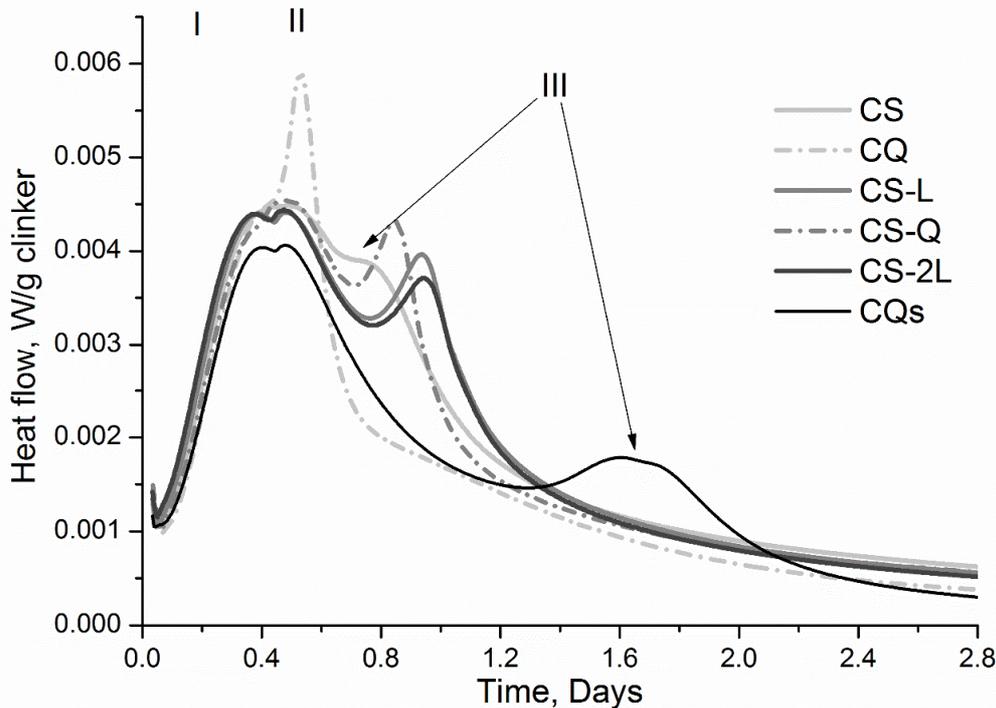
244

245 Figure 4 Effect of the slag-limestone interaction on the reaction rate of ternary slag
246 cements, by isothermal conduction calorimetry.

3.1.1. Clinker

248 The degree of hydration of the major clinker phases up to 180 days are shown in
249 Figure 5. A significant fraction of alite reacted in the first 12 hours in all mixes (Figure
250 5 a). The limestone-bearing cements showed higher degree of alite hydration
251 especially in the first 2 days irrespective of the limestone content. The presence of
252 quartz in the composite cements however had a negligible effect on alite hydration
253 compared to limestone.

254 The belite reaction meanwhile, showed differences between the various samples
255 (Figure 5 a). Blend CQ consistently showed a higher degree of reaction of belite
256 compared to the composite slag cements with the difference becoming greater at
257 longer hydration time. Among the slag blends, less than 10% of belite reacted in the
258 first 7 days but reacted to different extents afterwards depending on the cement
259 composition. The lowest belite hydration was measured in blend CS. The reacted
260 belite contents in the limestone-bearing samples were between those of sample CS
261 and CQ, while sample CS-Q showed belite levels similar to those seen in sample CS
262 for the first 7 days of hydration, but falling in line with those of the limestone-bearing
263 mixes after this. This is consistent with the observations reported elsewhere [35, 36].
264 Notwithstanding, significant proportions of unreacted belite were still present in the
265 various mixes even after 180 days. The hydration of C_3A and C_4AF shown in Figure
266 5 (b) were similar among the slag blends but both were slightly accelerated in the
267 binary quartz mix, CQ.

10
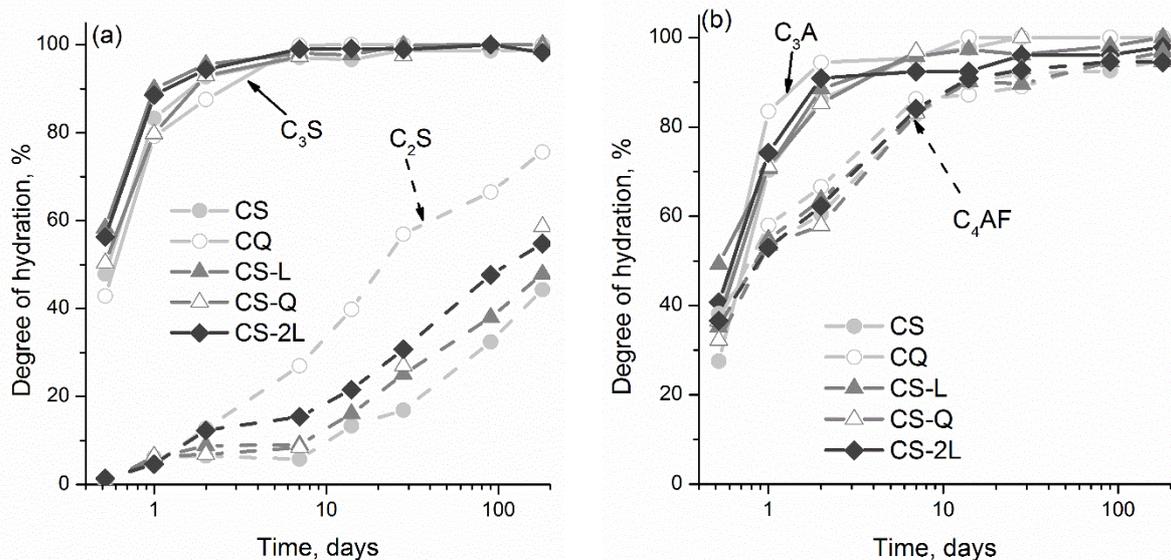
Figure 5 Effect of the slag-limestone interaction on the residual (a) C_3S and C_2S and (b) C_3A and C_4AF content in composite slag cements. Note that CQ contained no additional sulphate. The errors in the measurement was ± 2 %. Solid lines (a) C_3S, (b) C_3A and dashed lines (a) C_2S, (b) C_4AF.

268

3.1.2. Slag

270 Using the procedures described elsewhere [18, 36], the chemical shrinkage and heat
271 due to slag hydration (i.e. after discounting the filler effect) in the blends were
272 extracted, with the results shown in Figure 6 (a and b). Both techniques indicated
273 active hydration of slag from early ages in all investigated systems. The noise in the
274 shrinkage and calorimetry data in the first ~ 15 hours or so arose from differences in
275 the filler effects of slag and quartz on the silicate and aluminate reactions but did not
276 influence the overall hydration trends.

277 The chemical shrinkage and calorimetry methods are however semi-quantitative and
278 require calibration in order to estimate the actual degree of reaction of slag [18]. Two
279 independent methods, implementation of a PONKCS phase for GGBS in the Rietveld
280 refinement of XRD and BSEM/IA, were subsequently used to quantitatively measure
281 the degree of slag hydration. The results from each approach are presented in Figure
282 6 (c and d). Slag hydration was greater in the limestone-containing cements at all
283 ages. However, the Rietveld/PONKCS method has an error of ± 2%, thus the effects
284 at early ages cannot be definitely stated. Backscattered SEM/IA is also known to
285 overestimate the hydration degree at early ages due to resolution for particles under
286 2 µm [18, 36, 37]. By 1 day, the degree of slag hydration was about 25%. This is
287 similar to values reported elsewhere for slags of similar composition [18, 36], but
288 greater than those reported by Snellings *et al.* [38]. The enhanced reaction of slag in
289 the presence of limestone became clearer from 2 days onwards, with the effect
290 increasing slightly with increasing limestone content.
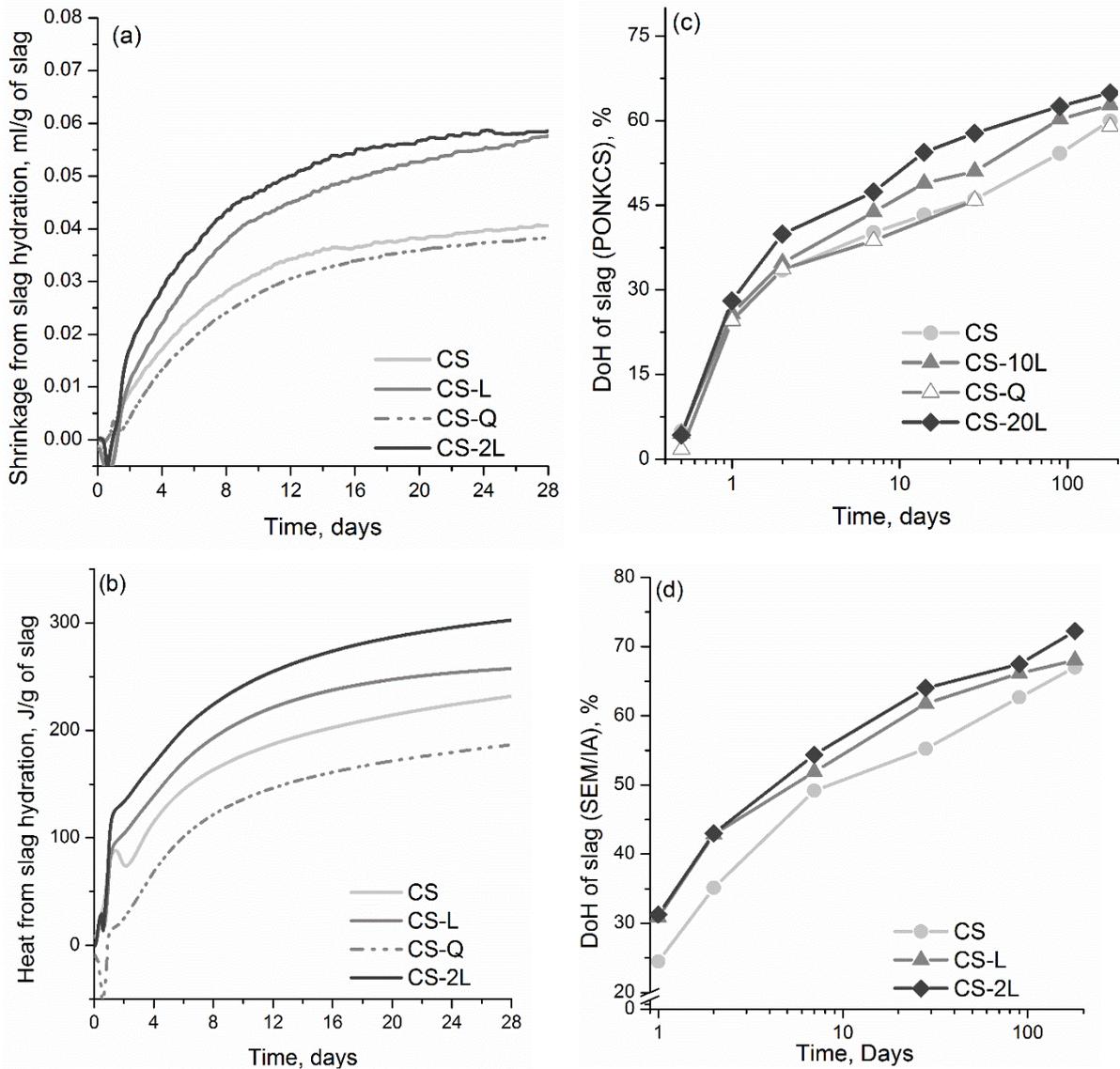
11

Figure 6 Effect of the slag-limestone interaction on slag hydration by (a) chemical shrinkage; (b) isothermal calorimetry; (c) QXRD/PONKCS and (d) SEM/IA

Despite the fact that the methods used here to follow slag hydration are characterised by the high measurement uncertainty, all of them indicate that slag hydration was enhanced in the presence of limestone. This led to increased slag reaction in the range of 5 -10% points.

3.1.3. Calcite

The previous sections have indicated that the presence of limestone did not only modify clinker hydration [7, 39] but also the hydration of slag. Consequently, the consumption of calcite in the ternary blends was investigated by thermal analysis and quantitative XRD. The derivative of the TG curves in Figure 7 (a and b) reveal a consistent reduction of the calcite content with hydration time thus confirming the

305 reaction of calcite. The trends from the derivative TG curves were consistent with the
306 QXRD data in Figure 7 (c). However, the reacted calcite was ~ 4 g per 100g of binder
307 after 180 days, thus indicating limited reaction of calcite irrespective of the initially
308 added content.
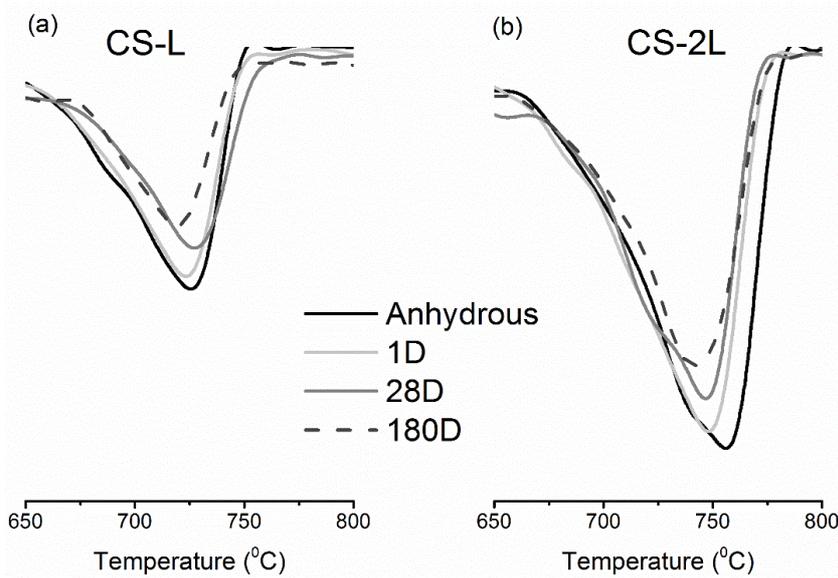
309
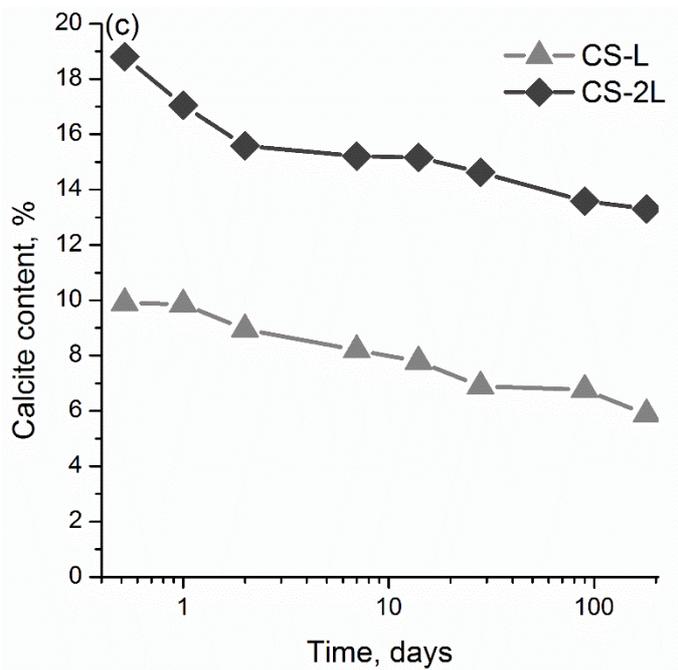
310

311 Figure 7 Consumption of calcite in ternary slag cements (a) at 10 % and (b) 20 %
312 limestone contents as measured by thermal analysis and (c) as a function of hydration
313 time, measured by QXRD. The error of measurement is ± 2 %.

## 3.2. Pore solution

315 The concentrations of calcium, aluminium, and sulphates in the pore solution from ~
316 30 minutes to 99 days of hydration are shown in Figure 8 (a - c) and other tabulated
317 in the appendix. The early stage reactions were characterised by a high calcium
318 concentration, which decreased steadily [40, 41] after 1 hour due to the precipitation

13

319 of hydrates. The concentrations in the limestone blends were higher (with the
320 exception of mix CS at the start of measurement). The lowest calcium concentration
321 was observed in mix CS-Q (Figure 8 a). However, the concentrations were similar for
322 all cements beyond 1 day.
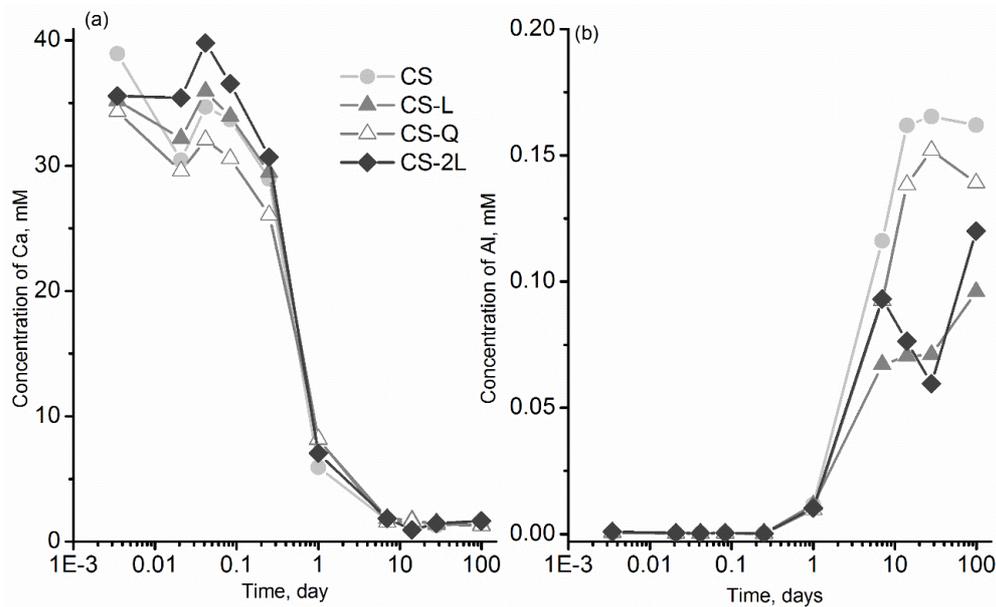
323
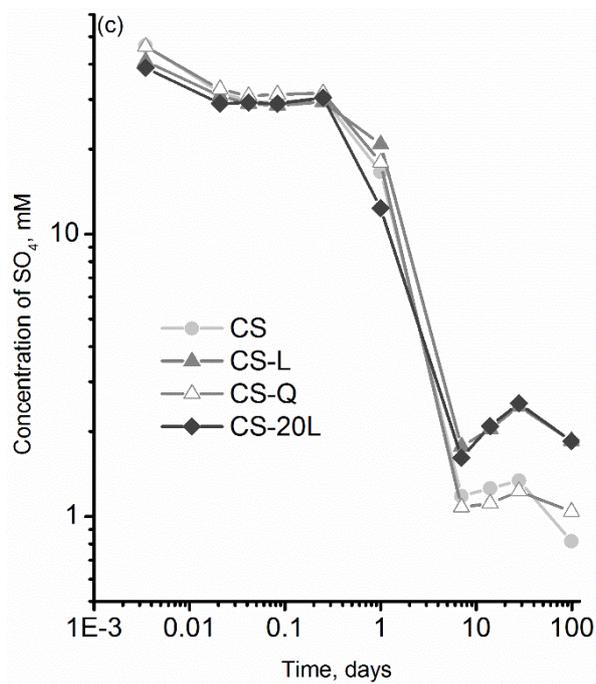
324

325 Figure 8 Measured total concentration of (a) calcium and (b) aluminum (c) sulphate in
326 the pore solution of composite slag cements measured by ICP-OES (≤1 day) and ion
327 chromatography (≥7 days).

328 Significant differences were observed in the aluminium concentration in the different
329 types of cement over the course of hydration (Figure 8 b). The levels were low over
330 the first 24 hours, irrespective of composition, and close to the detection limit of ICP-
331 OES, but rose beyond that. The trends show that the aluminium concentration in the

14

332 limestone containing cements was lower than the binary slag blend, mix CS.
333 Meanwhile, the aluminium concentration in the pore solution of mix CS-Q was slightly
334 lower than in the binary blend, but still considerably higher than in the limestone
335 bearing blends.

336 Sulphates (Figure 8 c) were detected in the pore solution with the concentration
337 decreasing rapidly in the first 1 hour as ettringite precipitated. The differences among
338 the various cements were slight, concentrations being lower in the limestone ternary
339 blends. The concentrations however stabilised until 6 hours but fell sharply afterwards
340 following depletion of bassanite and anhydrite. While the concentrations of calcium
341 and sulphates fell with hydration time, the pH increased, consistent with previously
342 reported data [11, 32].

3.3. Phase assemblages

343

344 In the investigated cements, C-S-H, portlandite, ettringite and carboaluminates were
345 the dominant hydrated phases. These were identified by TGA, XRD and SEM-EDX. It
346 should be noted that all composite cements, except mix CQ, contained 3 % total
347 sulphate content. The effects of mix composition on the development of each of these
348 phases with progressing hydration are considered in turn.

3.3.1. AFt

349

350 The presence of ettringite and C-S-H is evident from the DTG plots in Figure 10. After
351 1 day, more ettringite and C-S-H were formed in the limestone containing mixes
352 compared to those without, with the content increasing with the limestone content.
353 This trend was consistent at all ages, with the ettringite and C-S-H contents increasing
354 with hydration time.
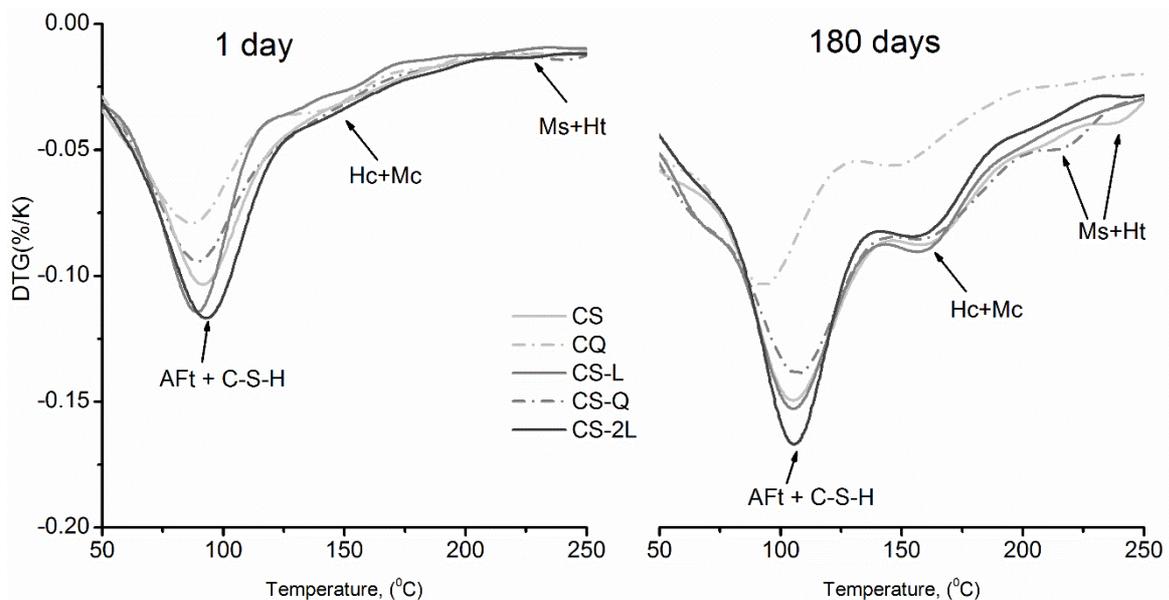
355

356 Figure 10 Evolution of the C-S-H, AFt and AFm phases in composite slag cements
357 after 1 and 180 days, as determined by TGA. AFt – ettringite, Ms –

monosulphoaluminate, Hc – hemicarboaluminate, Mc – monocarboaluminate, Ht – hydrotalcite.

Figure 11 indicates precipitation of ettringite after 12 hours of hydration. At this time, the reflection intensities were similar in all blends but increased significantly until 1 day. After this, the ettringite content was influenced by the cement composition, particularly by the presence of the additional limestone.
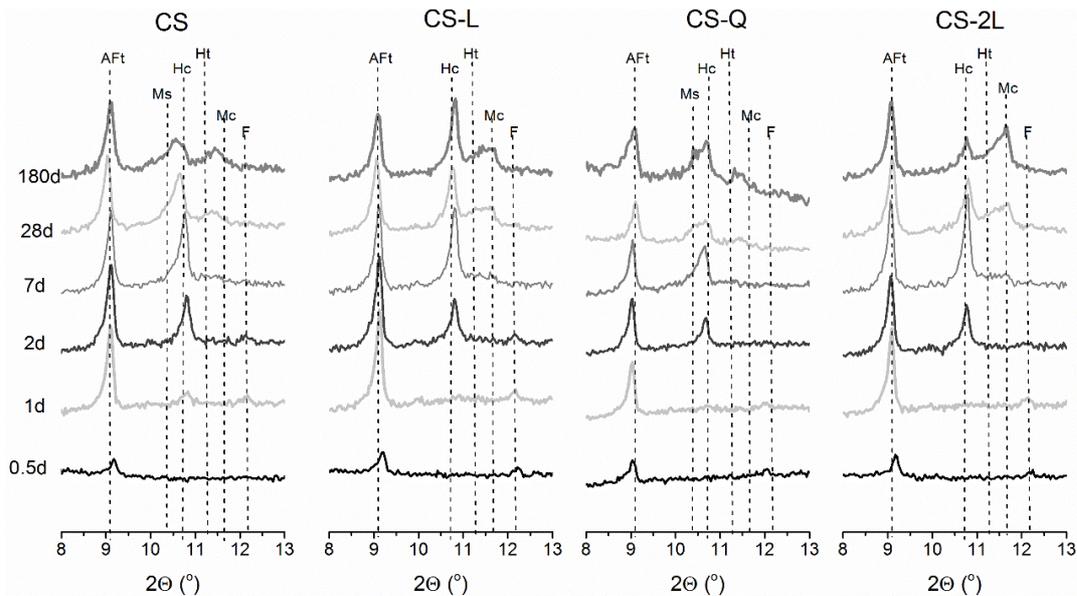
Figure 11 Effect of slag and limestone interaction on the sulphate and carbonate-bearing phase assemblages after 0.5, 1, 28 and 180 days hydration. AFt – ettringite, Ms – monosulphoaluminate, Hc – hemicarboaluminate, Mc – monocarboaluminate, Ht – hydrotalcite, F – ferrites.

The quantitative evaluation of the crystalline ettringite presented in Figure 12 indicates that, while the ettringite contents were unchanged in the limestone blends between 2 and 180 days, those in the mixes without limestone decreased steadily. Moreover, the ettringite content in the 20% limestone mix was slightly higher than that in the other blends. The ettringite content of the reference mix, CQ, was lowest because CQ contained less calcium sulphate.

3.3.2. Portlandite

The portlandite contents were similar in all cements after 1 day, as shown in Figure 12. From 2 days onwards, however, the CH content in mix CQ was consistently higher than in the composite slag cements. Those in the ternary limestone blends were lower, and increasingly so as the limestone content was raised from 10 to 20%.
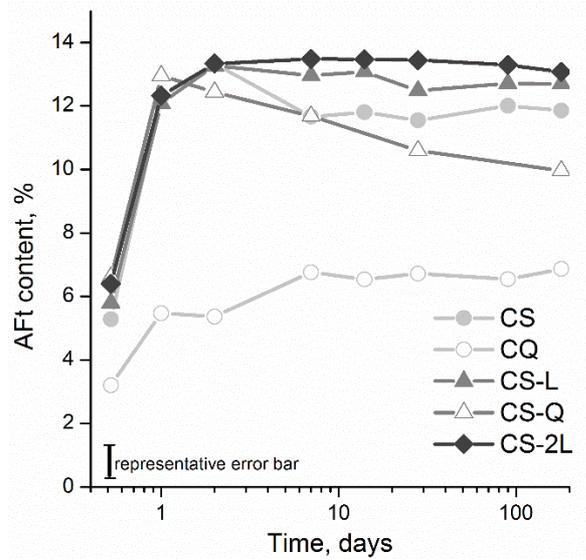
Figure 12 Effect of limestone on the ettringite content in ternary blends (XRD)
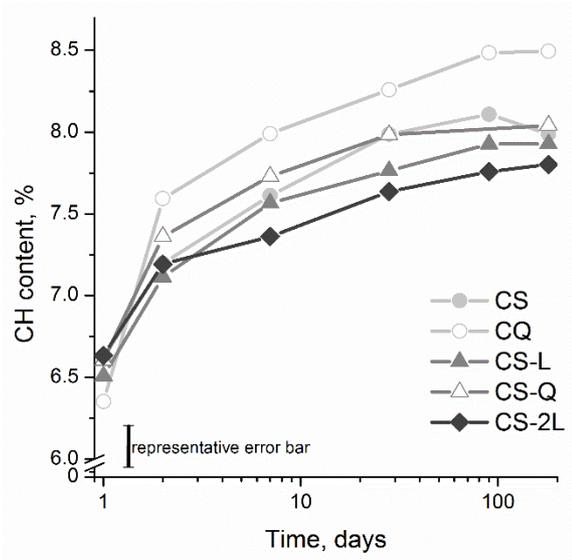
Figure 13 Effect of limestone on the evolution of portlandite in ternary slag blends (TG)

382

3.3.3. AFm

Figure 11 showed that hemicarboaluminate was the main carbonate bearing phase after the first 2 days of hydration but monocarboaluminate precipitated following the reaction of additional calcite. Monosulphoaluminate was however observed after 180 days in the blends without the additional limestone (see Figures 10 and 11). The latter being semi crystalline [42] meant it could not be quantified with any certainty.

The results from the Rietveld refinement of the crystalline hemi- and monocarboaluminate are presented in Figure 14. The hemicarboaluminate content increased gradually once sulphate was depleted, reaching a maximum of ~2 %. Monocarboaluminate was detected from 7 days, firstly in the limestone containing mixes as more calcite dissolved. The limestone content influenced the hemi/monocarboaluminate balance such that higher monocarboaluminate contents were noticed in the 20% limestone mixes.

17
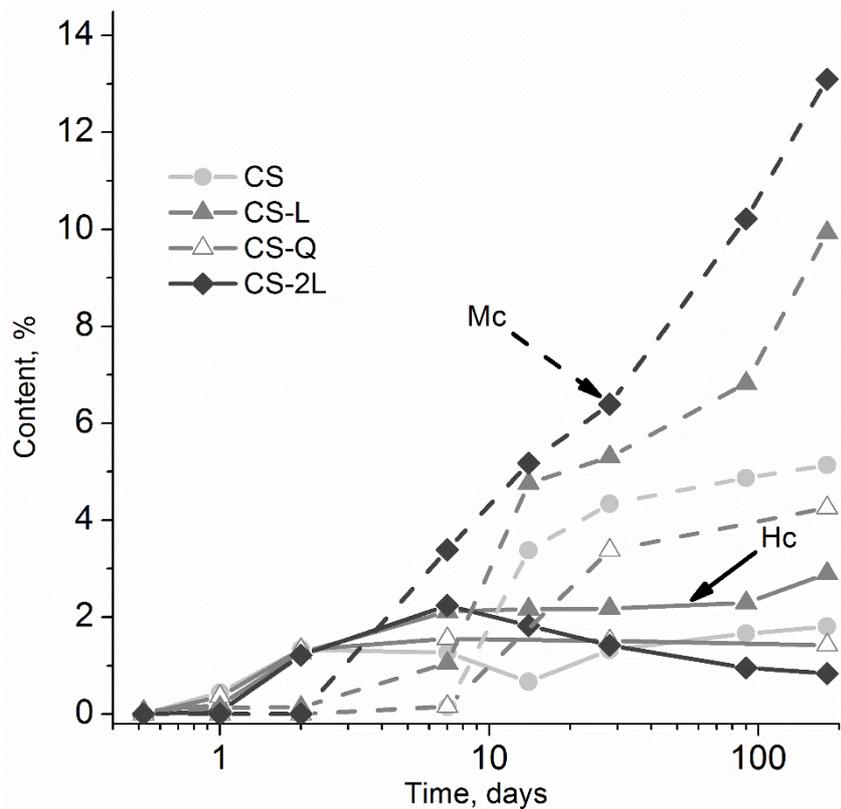
396

397 Figure 14 Effect of the slag-limestone interaction on the AFm content, analyzed by
398 Rietveld refinement. Solid lines denote trends in hemicarboaluminate and dashed
399 lines for monocarboaluminate.

3.3.4. C-S-H

401 The presence of limestone did not only modify the reaction kinetics but also the
402 contents of aluminate bearing hydrates and the pore solution as shown above.
403 Consequently, the composition of the C-S-H was investigated by SEM/EDS and the
404 results of the Al/Ca versus Si/Ca ratios are shown in Figure 15. The C-S-H Ca/Si
405 ratios differed slightly among the cements, being higher in the ternary limestone mixes;
406 increasing further after raising the limestone content to 20 %. The C-S-H Al/Si ratio
407 was, however, lower in the limestone ternary blends consistent with lower Al-
408 concentrations observed in the pore solution. There was no significant change in the
409 C-S-H Al/Si ratio with a change in the limestone content.

410
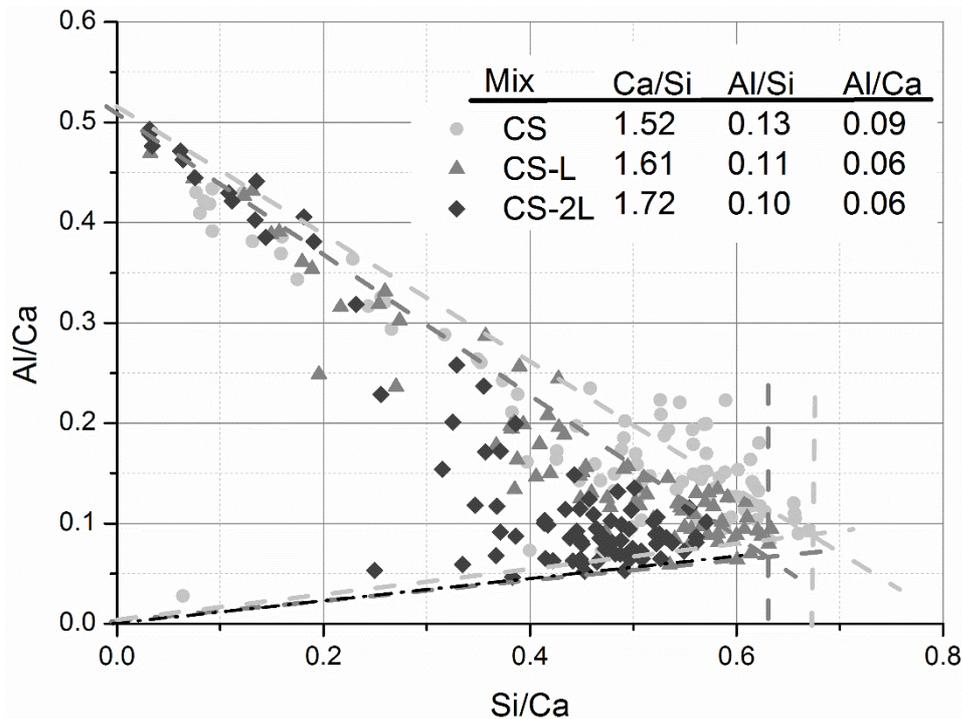
Figure 15 Effect of slag-limestone on the C-S-H composition after 180d, as analysed by SEM/EDX

3.3.5. Hydrotalcite

The hydrotalcite reflex is not clearly visible in Figure 11 because of its low crystallinity. However, its presence was confirmed by the TG data (Figure 10). Its presence could also be assumed within the hydrated slag rims, which could clearly be seen in SEM BSE images. Furthermore, SEM/EDS data may also be used to to determine the composition of the hydrated slag rim. The Mg/Al ratio of the hydrotalcite-like phase was taken as the slope of plots of Mg/Si against Al/Si [36] and shown in Figure 16.
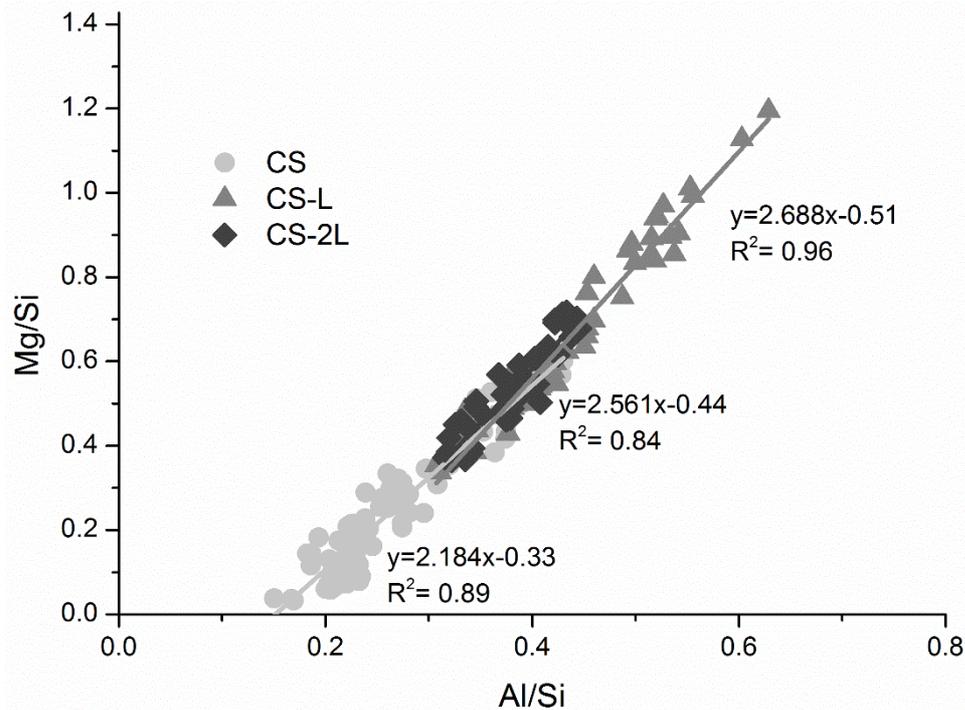
Figure 16 Effect of slag-limestone interaction on the composition of the slag rim after 180 d hydration

The Ca/Si and Al/Si ratios increased in the presence of limestone and further at higher limestone content. The hydrotalcite in the binary mix had an Mg/Al ratio of 2.2, while the limestone bearing mixes showed a ratio of 2.7 and 2.6, decreasing slightly with higher limestone content. The composition of the binary slag blend is consistent with the ratios reported elsewhere at similar replacement levels [43, 44].

3.4. Pore structure

Pore structures were characterised by the total pore volume and pore entry diameter, as determined by MIP, and the results are shown in Figure 17. In all mixes, the pore volume decreased and the critical pore diameters were refined as hydration progressed. The porosity evolution is similar for all of the samples containing slag. The similarity among the investigated slag-containing samples is further shown in Figure 18 which depicts the pore size distribution at 28 and 180 days.
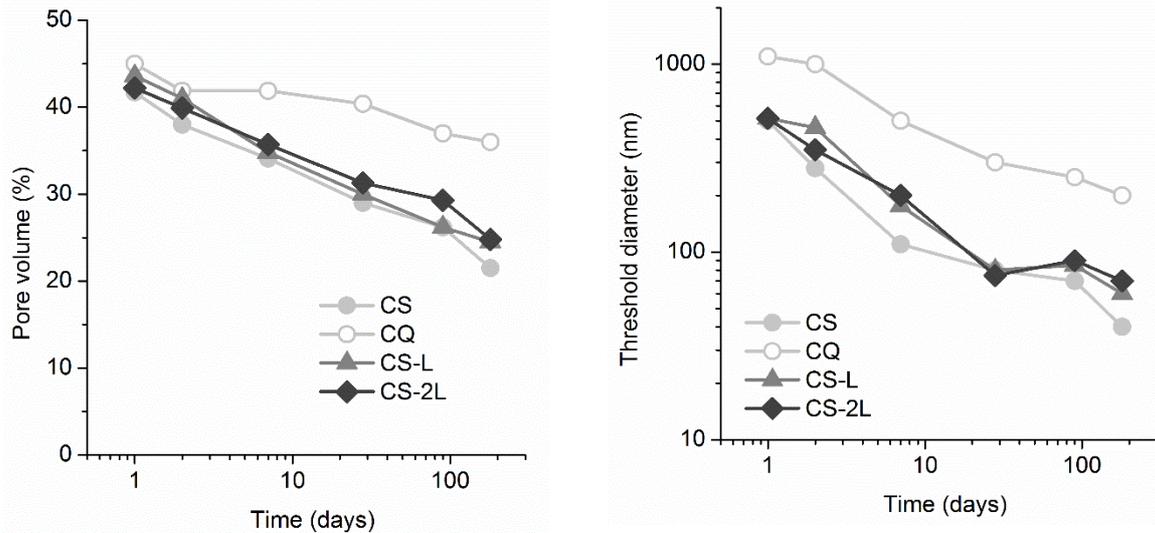
Figure 17 Effect of slag-limestone interaction on the (a) pore volume and (b) pore threshold diameter as measured by MIP.
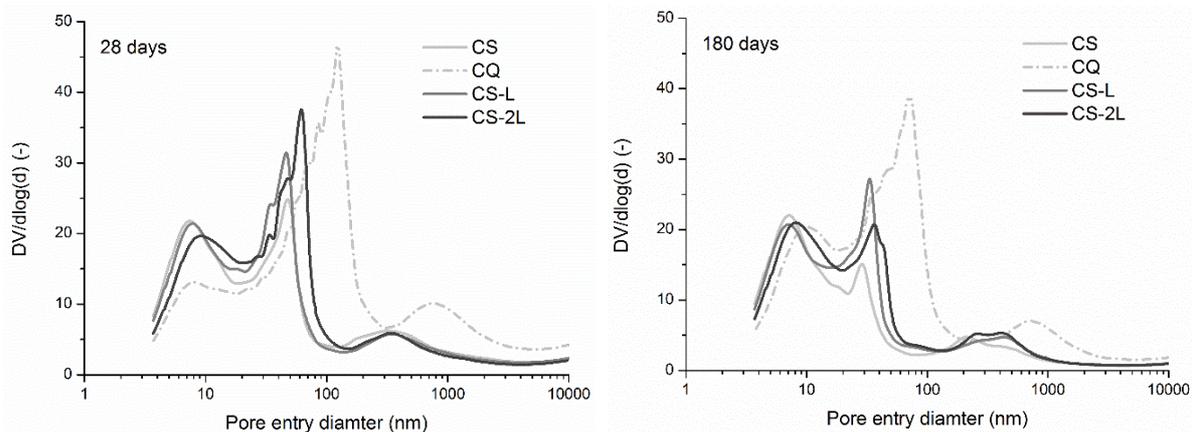
Figure 18 Effect of limestone on the accessible pores distribution as measured by MIP after 28 and 180 days of hydration

4. Discussion

The results demonstrate that the presence of limestone has an important impact on the kinetics of hydration of other constituents, on pore solution composition and hence on the hydrates formed. The filler effect, the availability of space for hydrates growth, and pore solution composition all influence the resultant microstructure and phase assemblage. The extent to which these are influential however depends on the hydration stage and are discussed in turn below.

4.1. Kinetics of hydration – filler effect

The acceleration of the clinker reaction is associated with the filler effect. In our results, the early hydration of the cement clinker (alite) was accelerated more in the presence of limestone and slag, when compared to the quartz. This is due to the specific effect for limestone which is a preferential nucleation surface compared to other SCMs [7].

21

452 The reaction degree of slag at early ages remains a topic of discussion [7, 20, 37].
453 The results presented in Figure 6 above point to the active hydration of slag, instead
454 of it being inert or merely a filler at early stages. For the given C_3A and sulphate
455 content, which was kept identical among the composite cements investigated, similar
456 sulphate depletion points [45] would be expected. However, the rate of reaction
457 (Figure 4) indicated that the presence of slag accelerated the sulphate depletion peak
458 (marked as III). It is probable that the aluminates dissolved from the slag contributed
459 to this effect. Additionally, dissolved slag increased the silicon concentration and
460 hence more C-S-H which can also adsorb sulphates. Indeed, the four complementary
461 techniques (Figure 6) point to considerable early-age hydration of slag.

462 Hydration at longer times is reported to be dependent on the space or water avaliable
463 for hydrate formation [25]. In this study, each of the composite cements contained 50
464 % clinker and were prepared with 0.5 w/b ratios. Therefore at the very early stages of
465 reaction, the water available for hydration (i.e. the dilution effect) would be similar and
466 hence can not fully explain differences in hydration among the investigated cements.
467 At longer hydration times however, hydrates will form around the most reactive
468 surfaces, including slag and clinker, and the availability of water and space has an
469 important role on belite, C_4AF and slag reaction [25].

470 This phenomenon is further explored in Figure 19 and 20. The free water content,
471 calculated as the difference between the initial water content (defined by the w/b) and
472 the bound water determined by TG, was similar for the three investigated slag-bearing
473 cements, at all hydration times, and lower than for the CQ sample. The MIP pore
474 volumes plotted against pore threshold diameters (in Figure 20) revealed that the
475 microstructures were also similar in the cements investigated. The decreasing
476 threshold with decreasing porosity up to the end of experiments demonstrated that
477 hydrate formation was not limited by microstructure fineness. Consequently, the
478 degree of slag hydration among the investigated samples cannot only be explained by
479 the available spaces for hydrate growth. Other factors must also account for some of
480 the differences in the hydration behaviour, for example, the pore solution composition.
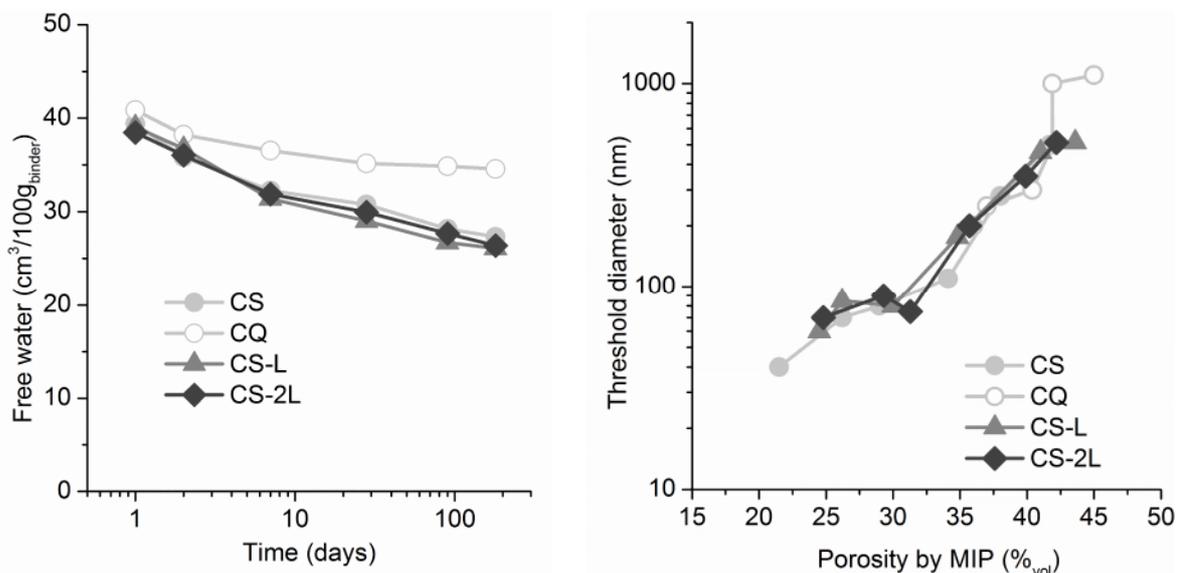
Figure 19 The effect of slag and limestone on the free water content in the investigated cements. Solid lines indicate the free water calculated as the difference between initial water content (defined by the w/b) and bound water measured by TG.

Figure 20 Correlation between MIP pore volume and pore threshold.

481

4.2. Kinetics of hydration – effect of pore solution

483 Pore solution concentrations depend on the kinetics of anhydrous phase dissolution
484 and of hydrate precipitation, as well as on the phase assemblage with which the pore
485 solution is in equilibrium. The application of thermodynamics to cement hydration has
486 shown that the hydrated phases are close to equilibrium with the pore solution [46,
487 47]. In the systems investigated, for a given alkali content, the calcium and aluminium
488 concentrations are limited mainly by the solubility of ettringite, AFm phases,
489 hydrotalcite, gypsum and portlandite. A simplified system was calculated using
490 thermodynamic modelling to demonstrate the impact of calcite on phase assemblage
491 as a function of the aluminate reacted. In the simplified scenarios, the Si-bearing
492 hydrates were excluded to facilitate the data comparison. Consequently, the
493 modelling comprises the effect of C_3A dissolution on the presence of portlandite,
494 calcium sulphate, MgO and calcite. The composition tested by the model was chosen
495 to test the possible phase assemblages (including Al-hydrates) in the investigated
496 samples. The results are given in Figure 21.

497

498

499

(a) No calcite
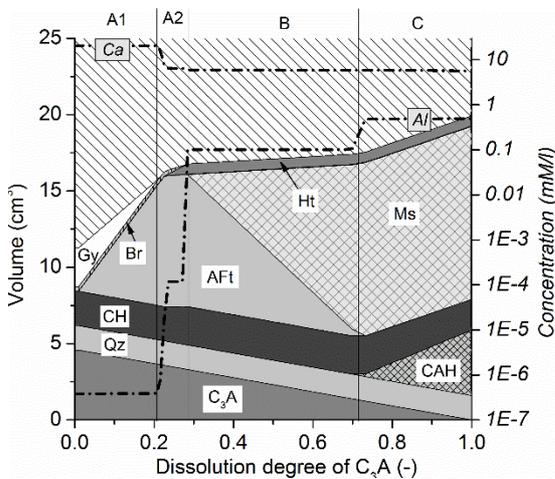
(b) With calcite
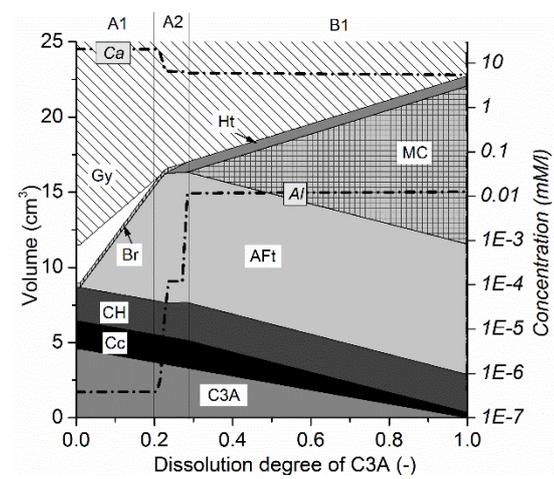
(c) Limited calcite
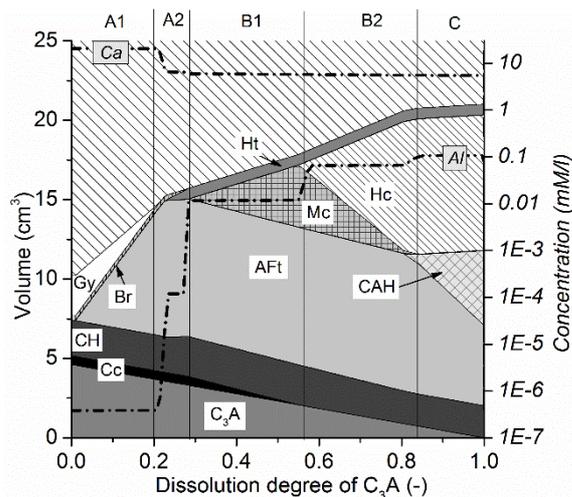
Figure 21 Modelling of the phase composition and Ca and Al concentrations of the simplified system (15 g C$_3$A, 5 g portlandite, 0.5 g MgO and 5 g anhydrite and 5 g calcite or quartz) influenced by the dissolution degree of aluminate phase. Three scenarios were investigated: (a) – no calcite, (b) – system saturated with calcite, (c) – not enough calcite to stabilise monocarboaluminate. Gy – Gypsum, Cc – calcite, CH portlandite, Br – brucite, Ht – hydrotalcite, AFt – ettringite, Mc – monocarboaluminate, Hc – Hemicarboaluminate, CAH – C4AH13, Ms – monosulfate. The centration of Al and Ca are shown with doted lines.

Modelling reveals that the phase assemblage and the presence of calcite have a pronounced impact on the Al and Ca concentrations:

- The aluminium concentration in the pore solution is very low in the presence of gypsum and ettringite, where high concentrations of Ca and sulphate are present due to the gypsum (Gy) solubility (assemblage A1). This corresponds to the early stage of hydration.
- Consumption of gypsum, with ettringite (AFt) being the primary sulphate-bearing phase, leads to a sudden marked increase in aluminium concentration and a slight drop in calcium ion concentration (assemblage A2).
- In the absence of calcite, the aluminium concentration rises further to the range of 0.1 mM/l, once monosulphoaluminate (Ms) phases are formed (assemblage B).
- However, in the presence of calcite, monocarboaluminate (Mc, assemblage B and B1) is formed instead of monosulphoaluminate. This results in lower Al concentrations, close to 0.01 mM/l. Insufficient calcite to stabilise the monocarboaluminate results in the precipitation of hemicarboaluminate (Hc) (assemblage B2), which further raises the Al concentration.
- For high C$_3$A/SO$_3$ ratios, the Al concentration is limited by the C$_4$AH$_{13}$ phase (CAH) to around 0.5 mM/l (assemblage C). This scenario is not applicable for the systems containing calcite since C$_4$AH$_{13}$ is not stable in the presence of calcite.

24

530 This simple model can explain the evolution of the Ca and Al pore solution
531 concentrations in the samples investigated. Although the measured aluminium
532 concentrations showed some variations, the limestone-bearing mixes showed
533 consistently lower aluminium concentrations than those without additional limestone.
534 This model also explains why the presence of calcite has little or no impact on the
535 early-age concentrations: which are dominated by the solubility product of gypsum
536 and ettringite. The XRD plots in Figure 11 indeed confirm monosulphoaluminate in the
537 absence of the additional limestone. The intensity of the latter was lower compared
538 to ettringite and hemicarboaluminate in samples CS and CQ consistent with the high
539 Al concentrations observed. In the limestone-bearing blends however, ettringite,
540 hemi- and monocarboaluminate were observed, consistent with the lower aluminium
541 concentrations measured in these samples. Both the measured concentrations and
542 the calculations are consistent with other thermodynamic predictions [1, 14]. A similar
543 lowering of Al concentrations in the presence of limestone has been previously
544 observed for binary Portland cement-limestone binders [11, 14].

545 Higher aluminium concentrations in the pore solution retard silicate dissolution [48,
546 49], as the sorption of aluminium on the surface sites of silicates slows down
547 dissolution. Consequently, lower aluminium levels in the pore solution can promote
548 the dissolution of glasses [49] and also of slag [50]. This was witnessed here by the
549 accelerated slag hydration in the limestone-bearing blends over sample CS-Q. The
550 inverse relationship between the Al concentration in the pore solution and the degree
551 of hydration of slag as determined by chemical shrinkage and the implementation of
552 the PONKCS phase for GGBS (Figure 22) confirms the significance of a lowering of
553 the aluminium concentration on slag hydration.
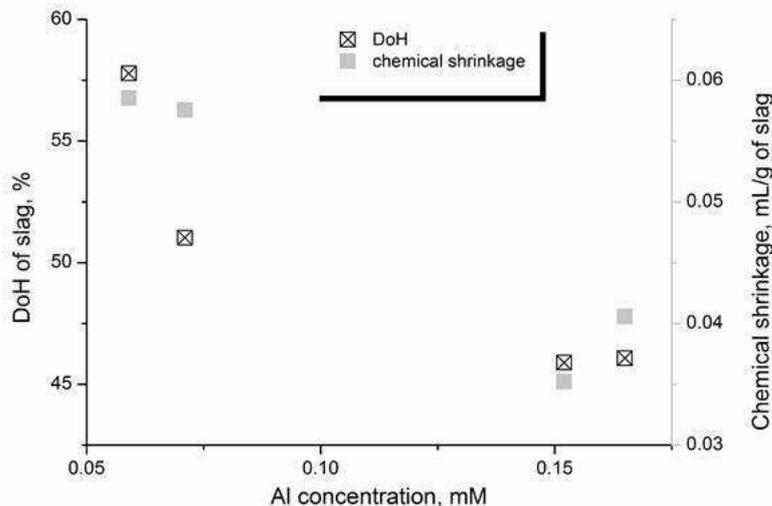
554

555 Figure 22 The relationship between Al concentration in the pore solution and chemical
556 shrinkage and degree of hydration of slag at 28 days. Note, there is ±2 % error
557 associated with the method for measuring the DoH of slag.

558

559 **4.3. Effect of limestone on phase assemblage**

560 Slightly greater ettringite contents (Figure 11 and 12) were observed in the limestone-
561 bearing blends compared to the binary blend, as expected from the literature [9, 10,
562 12] and predicted in Figure 21. These changes were significantly less pronounced
563 than for fly ash and calcined clay blended systems. This is partially caused by the
564 sulphate content being set to 3 % in this study, typical for industrial cement, resulting
565 in high AFt and low AFm contents. In many other studies, neat Portland cement has
566 been replaced by the supplementary cementitious materials without maintaining a
567 fixed SO_3 content [51, 52]

568 Aluminium uptake by C–S–H depends strongly on the aluminium concentrations in the
569 pore solution [53]. Consequently, the presence of limestone results in a decrease in
570 the C-S-H Al/Si ratio (Figure 15). Hence, more alumina is available for AFm formation,
571 as shown in Figures 14 and 21. The redistribution of alumina between C-S-H and
572 AFm phases has an impact on portlandite content, as less calcium is needed to form
573 the calcium-rich AFm phases as more Al is bound in the C-S-H resulting in less
574 portlandite. Hence, portlandite contents are lower as shown in Figure 13. Additionally,
575 this effect is intensified by the higher Ca/Si ratio of the C-S-H in the presence of
576 limestone.

577 The Mg/Al ratio of the hydrotalcite-like phase depends significantly on the chemical
578 composition of the investigated system [14, 36]. Unlike pure hydrotalcite with a Mg/Al
579 ratio of 3, a ratio closer to 2 is more common in slag cement blends [54]. In sample
580 CS, the measured Mg/Al ratio is with 2.2 close to that reported in the literature for the
581 similar systems [36]. However, in the presence of limestone, an important modification
582 is observed: the ratio increases up to 2.7, reflecting the sensitivity of hydrotalcite
583 composition to the hydrating environment. This agrees well with the above-described
584 modifications of the pore solution by calcite.

585

5 Conclusions

587 The presence of limestone has multiple effects on the hydration and phase
588 assemblage of ternary cements. Carbonate ions stabilise monocarboaluminate over
589 monosulphoaluminate or hemicarboaluminate, leading to an increased ettringite
590 content, as previously reported in the literature. However, this effect for slag blended
591 cements is not as pronounced as for fly ash and metakaolin containing systems.

592 Pore solution analysis and thermodynamic modelling reveal lower aluminium
593 concentrations in the pore solution when additional limestone is present. As high
594 aluminium concentrations slow down the dissolution of slags, the presence of
595 limestone accelerates slag hydration. A microstructural analysis reveals that additional
596 space for hydrate formation in the limestone-bearing samples compared to the
597 limestone free analogue, cannot be responsible for accelerated slag hydration, thus
598 confirming the impact of the pore solution.

599 Additionally, the presence of limestone modifies the composition of both the C-S-H
600 phase and of hydrotalcite. The C-S-H has lower Al/Si ratio in the presence of
601 limestone, while the hydrotalcite is characterised by a higher Mg/Al ratio. Both
602 phenomena can be explained by the lowering of the alumina concentration in the pore
603 solution in the presence of calcite.

604

609 **References**

610 [1] A. Schöler, B. Lothenbach, F. Winnefeld, M. Zajac, Hydration of quaternary
611 Portland cement blends containing blast-furnace slag, siliceous fly ash and limestone
612 powder, Cement and Concrete Composites, 55 (2015) 374-382.

613 [2] P. Mounanga, M. Khokhar, R. El Hachem, A. Loukili, Improvement of the early-age
614 reactivity of fly ash and blast furnace slag cementitious systems using limestone filler,
615 Materials and Structures, 44 (2011) 437-453.

616 [3] A. Arora, G. Sant, N. Neithalath, Ternary blends containing slag and
617 interground/blended limestone: Hydration, strength, and pore structure, Construction
618 and Building Materials, 102, Part 1 (2016) 113-124.

619 [4] K. De Weerdt, K.O. Kjellsen, E. Sellevold, H. Justnes, Synergy between fly ash and
620 limestone powder in ternary cements, Cement and Concrete Composites, 33 (2011)
621 30-38.

622 [5] M. Gesoğlu, E. Güneyisi, E. Özbay, Properties of self-compacting concretes made
623 with binary, ternary, and quaternary cementitious blends of fly ash, blast furnace slag,
624 and silica fume, Construction and Building Materials, 23 (2009) 1847-1854.

625 [6] G. Puerta-Falla, A. Kumar, L. Gomez-Zamorano, M. Bauchy, N. Neithalath, G.
626 Sant, The influence of filler type and surface area on the hydration rates of calcium
627 aluminate cement, Construction and Building Materials, 96 (2015) 657-665.

628 [7] E. Berodier, K. Scrivener, Understanding the filler effect on the nucleation and
629 growth of C-S-H, Journal of the American Ceramic Society, 97 (2014) 3764-3773.

630 [8] J.W. Bullard, H.M. Jennings, R.A. Livingston, A. Nonat, G.W. Scherer, J.S.
631 Schweitzer, K.L. Scrivener, J.J. Thomas, Mechanisms of cement hydration, Cement
632 and Concrete Research, 41 (2011) 1208-1223.

633 [9] T. Matschei, B. Lothenbach, F.P. Glasser, The AFm phase in Portland cement,
634 Cement and Concrete Research, 37 (2007) 118-130.

635 [10] T. Matschei, B. Lothenbach, F.P. Glasser, The role of calcium carbonate in
636 cement hydration, Cement and Concrete Research, 37 (2007) 551-558.

637 [11] B. Lothenbach, G. Le Saout, E. Gallucci, K. Scrivener, Influence of limestone on
638 the hydration of Portland cements, Cement and Concrete Research, 38 (2008) 848-
639 860.

640 [12] M. Zajac, A. Rossberg, G. Le Saout, B. Lothenbach, Influence of limestone and
641 anhydrite on the hydration of Portland cements, Cement and Concrete Composites,
642 46 (2014) 99-108.

643 [13] M. Antoni, J. Rossen, F. Martirena, K. Scrivener, Cement substitution by a
644 combination of metakaolin and limestone, Cement and Concrete Research, 42 (2012)
645 1579-1589.

646 [14] M. Ben Haha, B. Lothenbach, G. Le Saout, F. Winnefeld, Influence of slag
647 chemistry on the hydration of alkali-activated blast-furnace slag — Part II: Effect of
648 Al2O3, Cement and Concrete Research, 42 (2012) 74-83.

649 [15] X. Ke, S.A. Bernal, J.L. Provis, Controlling the reaction kinetics of sodium
650 carbonate-activated slag cements using calcined layered double hydroxides, Cement
651 and Concrete Research, 81 (2016) 24-37.

652 [16] CEMBUREAU, Environmental benefits of using alternative fuels in cement
653 production: A life-cycle approach, in, The European Cement Association, 2010.

654 [17] E. Gartner, Industrially interesting approaches to "low-CO2" cements, Cement and
655 Concrete Research, 34 (2004) 1489-1498.

656 [18] V. Kocaba, E. Gallucci, K.L. Scrivener, Methods for determination of degree of
657 reaction of slag in blended cement pastes, Cement and Concrete Research, 42 (2012)
658 511-525.

659 [19] R.W. Cheary, A.A. Coelho, J.P. Cline, Fundamental parameters line profile fitting
660 in laboratory diffractometers, J Res Natl Inst Stand Technol, 109 (2004) 1-25.

661 [20] B.H. O'Connor, M.D. Raven, Application of the Rietveld refinement procedure in
662 assaying powdered mixtures, Powder Diffraction, 3 (1988) 2-6.

663 [21] D. Jansen, F. Goetz-Neunhoeffer, C. Stabler, J. Neubauer, A remastered external
664 standard method applied to the quantification of early OPC hydration, Cement and
665 Concrete Research, 41 (2011) 602-608.

666 [22] D.C. Creagh, J.H. Hubbell, X-ray absorption (or attenuation) coefficients,
667 International Tables for Crystallography, C (2006) 220-229.

668 [23] C. Gallé, Effect of drying on cement-based materials pore structure as identified
669 by mercury intrusion porosimetry: A comparative study between oven-, vacuum-, and
670 freeze-drying, Cement and Concrete Research, 31 (2001) 1467-1477.

671 [24] H. Ma, Mercury intrusion porosimetry in concrete technology: tips in
672 measurement, pore structure parameter acquisition and application, Journal of porous
673 materials, 21 (2014) 207-215.

674 [25] E. Berodier, K. Scrivener, Evolution of pore structure in blended systems, Cement
675 and Concrete Research, 73 (2015) 25-35.

676 [26] M. Canut, M. Geiker, Pore structure and state of water of mixes with blended
677 cements, in: Proceedings of XIII ICCC International Congress on the Chemistry of
678 Cement, 2011.

679 [27] R.S. Barneyback Jr, S. Diamond, Expression and analysis of pore fluids from
680 hardened cement pastes and mortars, Cement and Concrete Research, 11 (1981)
681 279-285.

682 [28] D.A. Kulik, T. Wagner, S.V. Dmytrieva, G. Kosakowski, F.F. Hingerl, K.V.
683 Chudnenko, U.R. Berner, GEM-Selektor geochemical modeling package: revised
684 algorithm and GEMS3K numerical kernel for coupled simulation codes, Computational
685 Geosciences, 17 (2013) 1-24.

686 [29] T. Wagner, D.A. Kulik, F.F. Hingerl, S.V. Dmytrieva, GEM-Selektor geochemical
687 modeling package: TSolMod Library and data interface for multicomponent phase
688 models, The Canadian Mineralogist, 50 (2012) 1173-1195.

689 [30] T. Thoenen, D. Kulik, Nagra/PSI chemical thermodynamic database 01/01 for the
690 GEM-Selektor (V. 2-PSI) geochemical modeling code, PSI, Villingen, (2003).

691 [31] W. Hummel, U. Berner, E. Curti, F. Pearson, T. Thoenen, Nagra/PSI chemical
692 thermodynamic data base 01/01, Radiochimica Acta, 90 (2002) 805-813.

693 [32] B. Lothenbach, F. Winnefeld, Thermodynamic modelling of the hydration of
694 Portland cement, Cement and Concrete Research, 36 (2006) 209-226.

695 [33] T. Matschei, B. Lothenbach, F.P. Glasser, Thermodynamic properties of Portland
696 cement hydrates in the system CaO–Al 2 O 3–SiO 2–CaSO 4–CaCO 3–H 2 O,
697 Cement and Concrete Research, 37 (2007) 1379-1410.

698 [34] B. Lothenbach, T. Matschei, G. Möschner, F.P. Glasser, Thermodynamic
699 modelling of the effect of temperature on the hydration and porosity of Portland
700 cement, Cement and Concrete Research, 38 (2008) 1-18.

701 [35] V. Kocaba, Development and evaluation of methods to follow microstructural
702 development of cementitious systems including slags, in: Laboratoire des matériaux
703 de construction, EPFL, 2009, pp. 145.

704 [36] M. Whittaker, M. Zajac, M. Ben Haha, F. Bullergahn, L. Black, The role of the
705 alumina content of slag, plus the presence of additional sulfate on the hydration and
706 microstructure of Portland cement-slag blends, Cement and Concrete Research, 66
707 (2014) 91-101.

708 [37] M. Ben Haha, K. De Weerdt, B. Lothenbach, Quantification of the degree of
709 reaction of fly ash, Cement and Concrete Research, 40 (2010) 1620-1629.

710 [38] R. Snellings, A. Salze, K.L. Scrivener, Use of X-ray diffraction to quantify
711 amorphous supplementary cementitious materials in anhydrous and hydrated blended
712 cements, Cement and Concrete Research, 64 (2014) 89-98.

713 [39] S. Hoshino, K. Yamada, H. Hirao, XRD/Rietveld analysis of the hydration and
714 strength development of slag and limestone blened cement, Advanced Concrete
715 Technology, 4 (2006) 357-367.

716 [40] J.A. Larbi, A.L.A. Fraay, J.M.J.M. Bijen, The chemistry of the pore fluid of silica
717 fume-blended cement systems, Cement and Concrete Research, 20 (1990) 506-516.

718 [41] D. Ménétrier, I. Jawed, J. Skalny, Effect of gypsum on C3S hydration, Cement
719 and Concrete Research, 10 (1980) 697-701.

720 [42] D. Gastaldi, G. Paul, L. Marchese, S. Irico, E. Boccaleri, S. Mutke, L. Buzzi, F.
721 Canonico, Hydration products in sulfoaluminate cements: Evaluation of amorphous
722 phases by XRD/solid-state NMR, Cement and Concrete Research, 90 (2016) 162-
723 173.

724 [43] A.P. Barker, An electron optical examination of zoning in blastfurnace slag
725 hydrates: Part I. Slag cement pastes at early ages, Advances in Cement Research, 2
726 (1989) 171-179.

727 [44] J. Duchesne, M.A. Be´rube´, Effect of supplementary cementing materials on the
728 composition of cement hydration products, Advanced Cement Based Materials, 2
729 (1995) 43-52.

730 [45] D. Jansen, F. Goetz-Neunhoeffer, B. Lothenbach, J. Neubauer, The early
731 hydration of Ordinary Portland Cement (OPC): An approach comparing measured
732 heat flow with calculated heat flow from QXRD, Cement and Concrete Research, 42
733 (2012) 134-138.

734 [46] D. Damidot, B. Lothenbach, D. Herfort, F.P. Glasser, Thermodynamics and
735 cement science, Cement and Concrete Research, 41 (2011) 679-695.

736 [47] A. Schöler, B. Lothenbach, F. Winnefeld, M. Ben Haha, M. Zajac, H.-M. Ludwig,
737 Early hydration of SCM-blended Portland cements: A pore solution and isothermal
738 calorimetry study, Cement and Concrete Research.

739 [48] R.K. Iler, Effect of adsorbed alumina on the solubility of amorphous silica in water,
740 Journal of Colloid and Interface Science, 43 (1973) 399-408.

741 [49] R. Snellings, Solution-controlled dissolution of supplementary cementitious
742 material glasses at pH 13: The effect of solution composition on glass dissolution
743 rates, J Am Ceram Soc, 96 (2013) 2467–2475.

744 [50] P. Suraneni, M. Palacios, R.J. Flatt, New insights into the hydration of slag in
745 alkaline media using a micro-reactor approach, Cement and Concrete Research, 79
746 (2016) 209-216.

747 [51] W. Kunther, Z. Dai, J. Skibsted, Thermodynamic modeling of hydrated white
748 Portland cement–metakaolin–limestone blends utilizing hydration kinetics from 29Si
749 MAS NMR spectroscopy, Cement and Concrete Research, 86 (2016) 29-41.

750 [52] K. De Weerdt, M. Ben Haha, G. Le Saout, K.O. Kjellsen, H. Justnes, B.
751 Lothenbach, Hydration mechanisms of ternary Portland cements containing limestone
752 powder and fly ash, Cement and Concrete Research, 41 (2011) 279-291.

753 [53] B. Lothenbach, A. Nonat, Calcium silicate hydrates: Solid and liquid phase
754 composition, Cement and Concrete Research, 78, Part A (2015) 57-70.

755 [54] S.-D. Wang, K.L. Scrivener, Hydration products of alkali activated slag cement,
756 Cement and Concrete Research, 25 (1995) 561-571.

757

758

759 **Appendix**

760 Table A-1 Concentrations in the pore solution (mM) with hydration time

Mix ID	Time (d, hr)	Ca	Cl	K	Na	Si	S	pH
C2S1	0.003	38.90	-	76	15.2	0.027	46.50	13.04
	0.02	30.40	-	78	15.5	0.009	31.70	13.16
	0.04	34.70	-	80	15.8	0.006	29.60	13.23
	0.08	33.70	-	81	16	0.007	29.10	13.23
	0.25	28.90	-	85	17.7	0.015	30.20	13.18

	1.00	5.90	-	141	35.8	0.036	16.60	13.33
	7.00	1.72	0.49	158	55.31	0.034	1.18	13.32
	14.00	1.08	0.6	145	53.85	0.054	1.26	13.31
	28.00	1.28	0.51	143	56.76	0.053	1.34	13.31
	99.00	1.47	0.51	147	63.2	0.104	0.82	13.24
C2S1-10L	0.003	35.20	-	75	15.20	0.028	40.90	13.03
	0.02	32.20	-	79	15.30	0.015	30.90	13.11
	0.04	35.90	-	78	15.90	0.009	29.00	13.17
	0.08	33.90	-	79	16.10	0.011	28.60	13.15
	0.25	29.40	-	83	17.70	0.014	29.40	13.15
	1.00	8.10	-	103	22.30	0.043	20.80	13.20
	7.00	1.84	0.61	159	56.29	0.038	1.77	13.32
	14.00	1.71	0.62	152	54.67	0.038	2.04	13.31
	28.00	1.34	0.71	140	55.66	0.043	2.45	13.29
	99.00	1.33	0.82	143	62.81	0.106	1.85	13.24
C2S1-10Q	0.003	34.30	-	77	15.10	0.027	46.10	12.91
	0.02	29.60	-	78	15.50	0.011	32.60	13.03
	0.04	32.10	-	78	15.90	0.004	30.80	13.01
	0.08	30.60	-	80	16.20	0.005	31.30	13.03
	0.25	26.10	-	84	17.70	0.009	31.60	12.97
	1.00	8.20	-	114	33.70	0.011	17.90	13.27
	7.00	1.55	0.50	162	56.94	0.031	1.08	13.33
	14.00	1.60	0.48	161	57.24	0.033	1.11	13.34
	28.00	1.50	0.52	156	59.62	0.038	1.23	13.4
	99.00	1.25	0.54	144	63.28	0.104	1.04	13.27
C2S1-20L	0.003	35.60	-	67	15.30	0.038	38.70	12.87
	0.02	35.40	-	73	15.90	0.020	29.00	12.97
	0.04	39.80	-	75	16.10	0.014	29.20	13.03
	0.08	36.60	-	77	16.50	0.017	29.00	13.02
	0.25	30.70	-	80	17.70	0.020	30.40	12.99
	1.00	7.00	-	109	23.80	0.067	12.40	13.22
	7.00	1.80	0.50	158	53.70	0.035	1.60	13.25
	14.00	0.90	0.70	146	53.00	0.053	2.10	13.27
	28.00	1.40	0.70	145	54.00	0.036	2.50	13.27
	99.00	1.60	0.80	157	65.10	0.098	1.80	13.20

761